Received: 6 July 2017 | Revised: 11 October 2017 | Accepted: 17 October 2017

DOI: 10.1002/cmr.a.21402

ORIGINAL ARTICLE

WILEY

Analysis of the multi-echo spin-echo pulse sequence

Yuval Zur

GE Healthcare, Haifa, Israel

Correspondence
Yuval Zur, GE Healthcare, Haifa, Israel.
Email: yuval.zur@ge.com

Abstract

The multi-echo spin-echo sequence is a series of operators, referred to as periodic operators. Each periodic operator consists of a free rotation (no RF), a refocusing RF pulse, and another free rotation, identical to the first one. A preparation operator that precedes the periodic operators converts the equilibrium magnetization $\mathbf{M_z}$ into an initial magnetization $\mathbf{M_i}$. It is shown that a multi-echo sequence is equivalent to a simple rotation of the magnetization about a tilted axis. The component of $\mathbf{M_i}$ along the rotation axis is stationary and provides a stable signal, denoted pseudo steady-state. The perpendicular component rotates and eventually dephases. Using this model, we derive analytic expressions to the signal for different preparation operators, and show how to align $\mathbf{M_i}$ with the rotation axis such that the signal is maximized. A simple and efficient algorithm is presented to calculate the Fourier coefficients of the magnetization during the sequence using the discrete Fourier transform. Finally, formulas of the echo signal when unavoidable phase errors are generated are derived. We show how to eliminate artifacts caused by these errors and restore the original image.

KEYWORDS

discrete Fourier transform, Fourier coefficients, multi-spin-echo sequence, phase errors, pseudo steady-state

1 | INTRODUCTION

In this work, we shall analyze the multi-echo spin-echo sequence as shown in Figure 1. It is known in imaging as RARE,[1] Fast Spin Echo (FSE), or Turbo Spin Echo (TSE). It consists of a set of N periodic operators $\mathbf{R_p}$, preceded by an initial magnetization $\mathbf{M_i}$ which is generated by a preparation operator $\mathbf{R_{prep}}$ from the equilibrium magnetization $\mathbf{M_z}$. Each periodic operator consists of a rotation around the z-axis by ϕ radians, an RF pulse with flip angle θ, and another rotation around the z-axis by ϕ radians. The flip angles θ can vary from one periodic operator to another. An echo signal is acquired between 2 adjacent periodic operators. In NMR imaging, the phase ϕ is generated by gradients, but our analysis also hold for position-independent ϕ. The multi-spin-echo sequence was analyzed extensively in the literature using the Extended Phase Graph (EPG) algorithm.[2-9] Le Roux and Hinks[10] used a similar algorithm to calculate echo amplitudes, and devised an algorithm to stabilize the echoes at the beginning of the echo train.

It is well known[7,8] that the magnetization $M(\phi)^{(n)}$ after n periodic operators is a finite linear combination of $\exp(ik\phi)$, where k is an integer (see Equation (14)). The coefficients of this linear combination are called "Fourier coefficients" because they are calculated using the discrete Fourier transform of $M(\phi)^{(n)}$ as shown in Equation (16) below. The EPG algorithm tracks individual Fourier coefficients during the evolution of the magnetization along the echo train. In this work, we use a different approach and analyze the multi-echo sequence as a stack of periodic operators. This approach provides new insights, and complements the EPG analysis. To improve clarity and simplify the analysis, we use a vector model to describe the evolution of the magnetization. In some cases (eg, Equations (27), (32) and (D6)), the solution is given in terms of a simple numerical integral, rather than a complicated analytic expression.

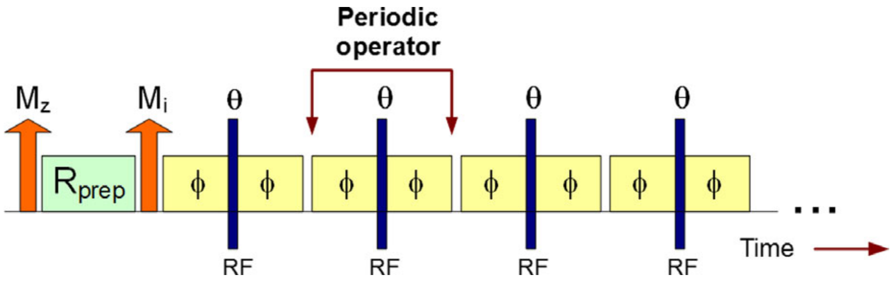

FIGURE 1 The multi-echo pulse sequence: N periodic operators are preceded by a prep operator $\mathbf{R_{prep}}$ that converts M_z to $\mathbf{M_i}$

In the first section, we show that the multi-echo sequence is equivalent to a simple rotation about a tilted axis. Consequently, the component of $\mathbf{M_i}$ which is aligned with the rotation axis remains unchanged, giving rise to a pseudo steady-state (PSS) signal.[5] The component of $\mathbf{M_i}$ which is perpendicular to the rotation axis rotates and eventually de-phases. Due to its simplicity, the evolution along the echo train (neglecting relaxation) can be calculated analytically, and analytic expressions for some Fourier coefficients of the magnetization are provided. Based on this analysis, an efficient algorithm using the discrete Fourier transform is presented to compute the Fourier coefficients of the magnetization. In the next section, we calculate the PSS and echo signal for some given initial magnetization $\mathbf{M_i}$. Then, we show how to design $\mathbf{R_{prep}}$ such that $\mathbf{M_i}$ is aligned with the rotation axis and the signal for a given flip angle θ is maximized. In the last section, this vector model is used to provide closed form formulas for the signal in case of a phase error between the excitation pulse of $\mathbf{R_{prep}}$ and the first periodic operator, ie, when the Carr-Purcell Meiboom-Gill (CPMG) condition[11,12] is violated. A method to correct this error is provided.

Alsop[13] also presented an analysis of the multi-echo sequence and derived the PSS signal $S = \sin(\theta/2)$ in Equation (19b) below (see (4), (5) and (6) in reference.[13]) Lukzen et al[14] derived analytic approximations to the pseudo steady-state signal and echo amplitudes without relaxation and later extended it and included relaxation and off-resonance.[15] The drawbacks of these derivations are: (i) the equations are difficult to evaluate because series expansions and integral evaluations are required; (ii) the approximate expressions for echo amplitudes without relaxation (reference (14) equation (27) and reference (15) equation (36)) converge to the exact solution (Equation (20)) after 8-10 echoes where the transient term $\boldsymbol{I}^{(n)}$ in Equation (20) is already close to zero.

2 | THEORY

The multi-echo pulse sequence is shown in Figure 1 with N periodic operators preceded by the preparation operator $\mathbf{R_{prep}}$. Without loss of generality, all RF pulses are in the x-axis. If relaxation is ignored, the periodic operator is a sequence of pure rotations. If an operator $\mathbf{R}$ is a rotation or a set of rotations of the magnetization vector, the axis and angle of rotation fully characterize $\mathbf{R}$, because the magnitude of the vector is preserved. Since only 2 parameters are needed to characterize $\mathbf{R}$, it can be described by a 2 × 2 unitary matrix

$$\mathbf{R} = \begin{pmatrix} \alpha & -\beta^* \\ \beta & \alpha^* \end{pmatrix}$$

where α and β are called the Cayley-Klein parameters (equations (1) and (2) in reference (16)). We prefer this notation over 3 × 3 rotation matrices because it simplifies the calculations. If α and β are known, one can calculate the equivalent 3 × 3 rotation matrix using the matrix located between equations (4) and (5) in reference.[16] If the initial magnetization is M_z, the final magnetization is given by equations (5) and (6) in reference.[16] The Cayley-Klein parameters α and β of a rotation $\mathbf{R}$ are calculated from the rotation axis and the rotation angle around this axis using equations (1) and (2) in reference.[16]

$$\alpha = \cos\left(\frac{\psi}{2}\right) + in_z \cdot \sin\left(\frac{\psi}{2}\right) \tag{1a}$$

$$\beta = i\left(n_x + in_y\right) \cdot \sin\left(\frac{\psi}{2}\right) \tag{1b}$$

n_x, n_y, and n_z are the x, y, and z components of a unit vector along the rotation axis and ψ is the rotation angle around this axis. We define positive ψ a clockwise rotation because proton spins rotate in the clockwise direction.[16]

From Equation (1), the rotation matrix $\mathbf{R_P}$ of the periodic operator, with a rotation of ϕ around z ($n_z = 1$, $n_x = n_y = 0$) and an RF flip angle θ around x ($n_x = 1$, $n_y = n_z = 0$), is given by

$$\mathbf{R_P} = \begin{pmatrix} \exp\left(\frac{i\phi}{2}\right) & 0 \\ 0 & \exp\left(-\frac{i\phi}{2}\right) \end{pmatrix} \begin{pmatrix} C & iS \\ iS & C \end{pmatrix} \begin{pmatrix} \exp\left(\frac{i\phi}{2}\right) & 0 \\ 0 & \exp\left(-\frac{i\phi}{2}\right) \end{pmatrix} = \begin{pmatrix} Cz & iS \\ iS & Cz^{-1} \end{pmatrix} \tag{2a}$$

where $C = \cos\left(\frac{\theta}{2}\right)$, $S = \sin\left(\frac{\theta}{2}\right)$ and $z = \exp(i\phi)$. The Cayley-Klein parameters of $\mathbf{R_P}$ in (2a) are

$$\alpha_P = Cz; \qquad \beta_P = iS. \tag{2b}$$

The rotation operator $\mathbf{R_n}$ after n periodic operators $\mathbf{R_p}$ is

$$\mathbf{R_n} = \mathbf{R_P}^n = \begin{pmatrix} Cz & iS \\ iS & Cz^{-1} \end{pmatrix}^n. \tag{3}$$

The final α and β are

$$\begin{pmatrix} \alpha \\ \beta \end{pmatrix} = \mathbf{R_n} \cdot \mathbf{R_{prep}} \cdot \begin{pmatrix} 1 \\ 0 \end{pmatrix} \tag{4}$$

where $\mathbf{R_{prep}}$ is the 2×2 matrix of the preparation operator (Figure 1). The vector $[1, 0]^T$ in Equation (4) is the initial α and β, where M is the initial thermal equilibrium magnetization M_z. It is obtained by setting $\psi = 0$ in Equation (1). The transverse and longitudinal magnetizations after n periodic operators are given by Equations (5) and (6) in reference[16]:

$$M_{xy}^{(n)} = M_x + iM_y = 2\alpha^*\beta; \qquad M_z^{(n)} = \alpha\alpha^* - \beta\beta^*. \tag{5}$$

The rotation axis and rotation angle of $\mathbf{R_P}$ are determined from Equation (2) using Equation (1). The rotation axis, a unit vector with components n_x, n_y, and n_z, is given by

$$\frac{n_z}{n_x} = \frac{\mathrm{imag}(\alpha_P)}{\mathrm{imag}(\beta_P)} = \frac{C \cdot \sin(\phi)}{S} \tag{6a}$$

$$n_y = \frac{-\mathrm{real}(\beta_P)}{\sin(\frac{\psi}{2})} = 0 \tag{6b}$$

imag() and real() are the imaginary and real part, respectively.

Using (6), the rotation axis of $\mathbf{R_P}$ is a unit vector aligned with the 3-components vector $\mathbf{V_A}$

$$\mathbf{V_A} = [1, 0, \lambda]^T \quad \text{where } \lambda \equiv \frac{C \cdot \sin(\phi)}{S}. \tag{7}$$

The rotation angle ψ in the clockwise direction around $\mathbf{V_A}$ is

$$\cos\left(\frac{\psi}{2}\right) = \mathrm{real}(\alpha_P) = C\cos(\phi); \quad \sin\left(\frac{\psi}{2}\right) = \frac{S}{n_x} = S\sqrt{1+\lambda^2}. \tag{8}$$

From (8)

$$\exp\left(i\frac{\psi}{2}\right) = \cos\left(\frac{\psi}{2}\right) + i\sin\left(\frac{\psi}{2}\right) = C\cos(\phi) + iS\sqrt{1+\lambda^2}. \tag{9a}$$

From (9a)

$$\exp(in\psi) = \left[\exp\left(i\frac{\psi}{2}\right)\right]^{2n} = \left[C\cos(\phi) + iS\sqrt{1+\lambda^2}\right]^{2n}. \tag{9b}$$

The rotation angle ψ is:

$$\psi = 2 \cdot \mathrm{angle}\left(C\cos\phi, S\sqrt{1+\lambda^2}\right) \tag{9c}$$

where “angle” in (9c) is the phase angle of a complex number Z in the $[-\pi, \pi]$ range defined as

$$\text{phase angle of } Z \equiv \text{angle}\ (\mathrm{real}(Z),\ \mathrm{imag}(Z)).$$

2.1 | Vector model

We shall now calculate the magnetization $\mathbf{M}^{(n)} = [M_x, M_y, M_z]^T$ after n periodic operators and a given initial magnetization $\mathbf{M_i}$. This is done in 3 steps: (i) write $\mathbf{M_i}$ as a vector sum of 2 vectors: $\mathbf{M_A}$ along $\mathbf{V_A}$ and a vector $\mathbf{M_P}$ perpendicular to $\mathbf{V_A}$; (ii) during the application of $\mathbf{R_n}$, $\mathbf{M_A}$ does not change while $\mathbf{M_P}$ rotates by $n\psi$ radians in a plane perpendicular to $\mathbf{V_A}$; (iii) add $\mathbf{M_A}$ to the rotated $\mathbf{M_P}$ to obtain the final magnetization $\mathbf{M}^{(n)}$. This is demonstrated in Figure 2. $\mathbf{M_P}$ and $\mathbf{M_A}$ fulfill 3 conditions:

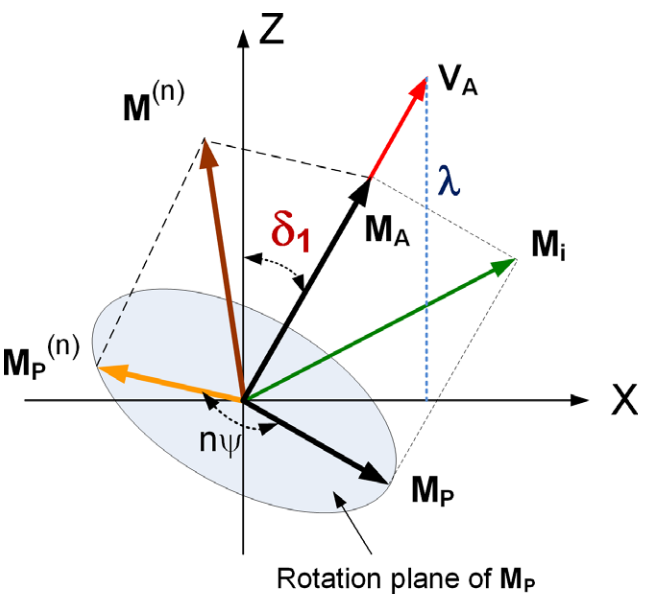

FIGURE 2 $\mathbf{M_i}$ is decomposed to 2 perpendicular vectors $\mathbf{M_P}$ and $\mathbf{M_A}$, where $\mathbf{M_A}$ is collinear with the rotation axis $\mathbf{V_A}$ in Equation (7). $\mathbf{M_A}$ is in the XZ plane at an angle Θ = angle (1, λ) with the x-axis and $\delta_1 = 90° -$ angle(1, λ) with the z-axis. n periodic operators rotate $\mathbf{M_P}$ by $n\Psi$ radians in a plane perpendicular to $\mathbf{M_A}$. The final magnetization $\mathbf{M^{(n)}}$ is a vector sum of $\mathbf{M_P^{(n)}}$ (the rotated $\mathbf{M_P}$), and $\mathbf{M_A}$

(i) $\mathbf{M_P} \bullet \mathbf{M_A} = 0$; (ii) $\mathbf{M_P} + \mathbf{M_A} = \mathbf{M_i}$; (iii) $\mathbf{M_A}$ is collinear with $\mathbf{V_A}$. The symbol • is the scalar product of 2 vectors and $\mathbf{M_i} = \left[M_{ix}, M_{iy}, M_{iz}\right]^T$. If $\mathbf{M_i}$ is known, $\mathbf{M_P}$ and $\mathbf{M_A}$ that fulfill these conditions are determined uniquely:

$$\mathbf{M_A} = [1, 0, \lambda]^T \cdot A; \quad \mathbf{M_P} = [-\lambda, 0, 1]^T \cdot B + [0, M_{iy}, 0]^T \tag{10}$$

$$\text{where } A = \frac{M_{ix} + \lambda M_{iz}}{1 + \lambda^2} \quad \text{and} \quad B = \frac{M_{iz} - \lambda M_{ix}}{1 + \lambda^2}.$$

$\mathbf{M_A}$ in (10) depends on $\mathbf{M_i}$ and the flip angle θ through the parameter λ. The pseudo steady-state (PSS) magnetization $\mathbf{M_A}$ (collinear with $\mathbf{V_A}$) is the projection of $\mathbf{M_i}$ on the rotation axis direction $\mathbf{V_A}$. Therefore, if $\mathbf{M_i}$ is collinear with $\mathbf{V_A}$, $\mathbf{M_A}$ is maximal. On the other hand, if $\mathbf{M_i}$ is perpendicular to $\mathbf{V_A}$, the pseudo steady-state magnetization $\mathbf{M_A}$ is zero.

The magnetization $\mathbf{M}^{(n)}$ after n periodic operators is calculated in Appendix A. The 3 × 3 rotation matrix $\mathbf{R^{(n)}}$ after n periodic operators is given by Equation (A2), and the total magnetization $\mathbf{M}^{(n)}$ by Equation (A5). This simplifies the calculation of $\mathbf{M}^{(n)}$ to an evaluation of a 3 × 3 matrix. (A2) holds only if the flip angle θ is the same for all RF pulses and relaxation is neglected.

Our goal is to maximize $\mathbf{M_A}$ and minimize (or even zero) $\mathbf{M_P}$. This occurs if $\mathbf{R_{prep}}$ tilts M_z to the direction of $\mathbf{V_A}$ for all ϕ, such that $\mathbf{M_P} = 0$. From Equation (10)

$$\mathbf{M_P} = 0 \quad \Rightarrow \quad M_{iz} = \lambda M_{ix} \quad \text{and } M_{iy} = 0. \tag{11a}$$

If TR > T_1, $M_{ix}^2 + M_{iz}^2 = M_0 = 1$. Using (11a):

$$M_{ix} = \frac{1}{\sqrt{1+\lambda^2}}; \quad \mathbf{M}_{\mathrm{Amax}} = \frac{[1, 0, \lambda]^T}{\sqrt{1+\lambda^2}} \tag{11b}$$

$\mathbf{M_{Amax}}$ is the maximum pseudo steady-state magnetization for a given ϕ and θ. If $\mathbf{M_P} \neq 0$, then $|\mathbf{M_A}| < |\mathbf{M_{Amax}}|$. Define

$$R_{\mathrm{MA}} \equiv \frac{|\,\mathbf{M_A}\,|}{|\,\mathbf{M_A max}\,|} = |\,A\,| \cdot \sqrt{1+\lambda^2} = \frac{|\,M_{ix} + \lambda M_{iz}\,|}{\sqrt{1+\lambda^2}} \tag{11c}$$

where $0 \le R_{\mathrm{MA}} \le 1$. $R_{\mathrm{MA}} = 1$ indicates maximal $\mathbf{M_A}$ and zero $\mathbf{M_P}$. Therefore, an optimal $\mathbf{R_{prep}}$ generates $\mathbf{M_i}$ with the largest possible R_{MA}. Below we shall optimize $\mathbf{R_{prep}}$ by maximizing R_{MA}. Equation (11) was originally derived by Alsop (equation (6) in reference (13)).

2.2 | Relaxation

In a real experiment, T_1 and T_2 relaxation cannot be neglected, so the periodic operator can no longer be represented by pure rotations. The nth periodic operator in a pulse sequence with N RF pulses operates on the $(n-1)$ magnetization vector $\boldsymbol{M}^{\mathbf{(n\text{-}1)}}$ to yield the nth magnetization vector $\mathbf{M^{(n)}}$. This is a product of 3 operators: (i) a rotation by ϕ around z plus T_1 and T_2 relaxation; (ii) an RF pulse of flip angle θ around x; (iii) another rotation by ϕ around z with T_1 and T_2 relaxation. The magnetization vector is $\mathrm{M} = \left[M_{xy} \;\; M_{xy}^* \;\; M_z\right]^T$ where $M_{xy} = M_x + iM_y$ and $M_{xy}^* = M_x - iM_y$. Starting from $\boldsymbol{M}^{\mathbf{(n\text{-}1)}}$, the magnetization $\mathbf{M_1}$ after the first rotation by ϕ and relaxation is

$$\begin{pmatrix} \mathbf{M_1} \end{pmatrix} = \begin{pmatrix} E_2\exp(-i\phi) & 0 & 0 \\ 0 & E_2\exp(i\phi) & 0 \\ 0 & 0 & E_1 \end{pmatrix} \begin{pmatrix} \mathbf{M^{(n-1)}} \end{pmatrix} + \begin{pmatrix} 0 \\ 0 \\ 1-E_1 \end{pmatrix}. \tag{12a}$$

Where $E_1 = \exp(-\tau/T_1)$, $E_2 = \exp(-\tau/T_2)$. τ is half the time between adjacent RF pulses. The RF operator is a rotation by the flip angle θ around x[16]:

$$\mathrm{RF} = \begin{pmatrix} (\alpha^*)^2 & -\beta^2 & 2\alpha^*\beta \\ -(\beta^*)^2 & \alpha^2 & 2\alpha\beta^* \\ -\alpha^*\beta^* & -\alpha\beta & \alpha^*\alpha - \beta^*\beta \end{pmatrix}. \tag{12b}$$

α and β are the Cayley-Klein parameters of a rotation around x (Equation (1)), $\alpha = \cos\left(\frac{\theta}{2}\right)$ and $\beta = i\sin\left(\frac{\theta}{2}\right)$. To obtain $\mathbf{M^{(n)}}$, $\mathbf{M_1}$ in (12a) is rotated by the RF operator in (12b) and then by the third operator, which is identical to the rotation and relaxation matrix in (12a):

$$\begin{pmatrix} \mathbf{M^{(n)}} \end{pmatrix} = \begin{pmatrix} E_2\exp(-i\phi) & 0 & 0 \\ 0 & E_2\exp(i\phi) & 0 \\ 0 & 0 & E_1 \end{pmatrix} \begin{pmatrix} \\ \mathbf{RF} \\ \\ \end{pmatrix} \begin{pmatrix} \mathbf{M_1} \end{pmatrix} + \begin{pmatrix} 0 \\ 0 \\ 1-E_1 \end{pmatrix}. \tag{12c}$$

We consolidate the operators in (12a) and (12c) and relate $\boldsymbol{M}^{\mathbf{(n\text{-}1)}}$ to $\mathbf{M^{(n)}}$ in a single Equation:

$$\begin{aligned} M_{xy}^{(n)}(\phi) = {} & E_2^2 e^{-2i\phi}(\alpha^*)^2 \cdot M_{xy}^{(n-1)} - E_2^2\beta^2 \cdot M_{xy}^{*(n-1)} \\ & + 2E_1E_2e^{-i\phi}\alpha^*\beta \cdot M_z^{(n-1)} + 2(1-E_1)E_2e^{-i\phi}\alpha^*\beta \end{aligned} \tag{13a}$$

$$
\begin{aligned}
M_z^{(n)}(\phi) = &-E_1E_2e^{-i\phi}\alpha^*\beta^*\cdot M_{xy}^{(n-1)} - E_1E_2e^{i\phi}\alpha\beta\cdot M_{xy}^{*(n-1)}\\
&+E_1^2(\alpha^*\alpha-\beta^*\beta)\cdot M_z^{(n-1)}\\
&+(1-E_1)E_1(\alpha^*\alpha-\beta^*\beta)+1-E_1.
\end{aligned}
\tag{13b}
$$

2.3 | Fourier representation

From (5), (13) and the EPG analysis,[3,5,7] it can be shown that $\mathbf{M^{(n)}}$ in sequence with N periodic operators can be written as a power series in z = exp ($i\phi$) with powers from $-2N$ to $2N$:

$$
M_{xy}^{(n)}(\phi)=\sum_{k=-2N}^{2N}A_k^{(n)}\cdot z^k;\qquad M_z^{(n)}(\phi)=\sum_{k=-2N}^{2N}B_k^{(n)}\cdot z^k \tag{14}
$$

A_k and B_k are ϕ independent complex numbers, called the Fourier coefficients of $\mathbf{M^{(n)}}$. If $M_{xy}^n(\phi)$ and $M_z^{(n)}(\phi)$ are known analytically (see below), A_k and B_k can be calculated by integration (reference (17) section 7.7):

$$
\begin{aligned}
A_k^{(n)} &= \frac{1}{2\pi}\int_{-\pi}^{\pi}M_{xy}^{(n)}\ (\phi)\ e^{-i\phi k}\ d\phi;\\
B_k^{(n)} &= \frac{1}{2\pi}\int_{-\pi}^{\pi}M_z^{(n)}(\phi)\ e^{-i\phi k}\ d\phi.
\end{aligned}
\tag{15a}
$$

When ϕ is generated by a gradient, all z^k with $k \neq 0$ in (14) de-phase and disappear, and $M_{xy}^{(n)}=A_0^{(n)}$ and $M_z^{(n)}=B_0^{(n)}$. From (15a), the nth sampled signal $M_{xy}^{(n)}$ referred to as the nth echo Echo(n) is

$$
\text{Echo}\ (n)=M_{xy}^{(n)}=A_0^{(n)}=\frac{1}{2\pi}\int_{-\pi}^{\pi}M_{xy}^{(n)}(\phi)\ d\phi. \tag{15b}
$$

In Appendix B, we show that Equation (15) can be simplified for pi-symmetric (pi-antisymmetric) functions and that only the pi-symmetric part of $M_{xy}^{(n)}$ contributes to the echo A_0.

The drawback of Equation (15) is that a continuous M (ϕ) is required to evaluate the integrals accurately. Alternatively, the $4N + 1$ coefficients A_k and B_k in Equation (14) can be computed by calculating $M_{xy}^{(n)}(\phi)$ and $M_z^{(n)}(\phi)$ in Equation (5) (no relaxation) or (13) (with relaxation) at discrete $4N + 1$ angles ϕ_j from 0 to 2π. Substitution of these $M_{xy}^{(n)}(\phi_j)$ and $M_z^{(n)}(\phi_j)$ in (14) is equivalent to solving a system with $4N + 1$ unknowns (A_k and B_k) with $4N + 1$ Equations. The solution $A_k^{(n)}$ and $B_k^{(n)}$ is very stable and simple (reference (18) section 8.1, reference (19) section 10.3) when ϕ_j is set to $4N + 1$ equally spaced angles ϕ_j from 0 to 2π, ie, $\phi_j=\frac{2\pi j}{4N+1}$ where j = 0 to $4N$, and is given by

$$
\begin{aligned}
A_k^{(n)} &= \frac{1}{4N+1}\sum_{j=0}^{4N}M_{xy}^{(n)}(\phi_j)\cdot\exp[-i\phi_j k]\\
&= \frac{1}{4N+1}\mathrm{DFT}\left(M_{xy}^{(n)}(\phi_j\right)
\end{aligned}
\tag{16a}
$$

$$
\begin{aligned}
B_k^{(n)} &= \frac{1}{4N+1}\sum_{j=0}^{4N}M_z^{(n)}(\phi_j)\cdot\exp[-i\phi_j k]\\
&= \frac{1}{4N+1}\mathrm{DFT}\left(M_z^{(n)}(\phi_j)\right)
\end{aligned}
\tag{16b}
$$

where DFT is the Discrete Fourier Transform with $4N + 1$ points. A MATLAB implementation of this algorithm to calculate $A_k{}^{(n)}$ and $B_k{}^{(n)}$ (with relaxation) for all k and all n between 1 and N is shown in Appendix C. This simple and efficient algorithm is about 3 times faster (measured with the MATLAB internal timer) than the EPG algorithm.[5,7]

Usually, we are only interested in the echo A_0. In this case, $M_{xy}^{(n)}(\phi)$ and $M_z^{(n)}(\phi)$ needs to be calculated only for $2N + 1$ equally spaced angles, ie, $\phi_j=\frac{2\pi j}{2N+1}$ with j = 0 to $2N$. There are not enough Equations (only $2N + 1$) to solve all A_k and B_k. As shown in reference (18) section 3.2, the DFT operator in (16a) with $2N + 1$ points provides linear combinations of A_k terms for $k \neq 0$ (aliasing), whereas A_0 for $k = 0$ remains intact. Similarly, (16b) with $2N + 1$ points provides linear combinations of B_k terms for $k \neq 0$, and B_0 remains intact. Therefore, A_0 and B_0 are calculated by a DFT with $2N + 1$ points and $k = 0$:

$$
\begin{aligned}
A_0^{(n)} &= \frac{1}{2N+1}\sum_{j=0}^{2N}M_{xy}^{(n)}(\phi_j)=\mathrm{mean}\left(M_{xy}^{(n)}\right);\\
B_0^{(n)} &= \frac{1}{2N+1}\sum_{j=0}^{2N}M_z^{(n)}(\phi_j)=\mathrm{mean}\left(M_z^{(n)}\right)
\end{aligned}
\tag{16c}
$$

where mean() in (16c) is the average of all $2N + 1$ values of M_{xy} (ϕ_j) and M_z (ϕ_j).

The analysis above assumes non-selective hard RF pulses and ignores off-resonance effects. This analysis and the computer program in Appendix C can be extended to slice-selective soft pulses, by calculating the b_1 waveforms of all the RF pulses, and dividing each waveform into piece-wise constant segments as in Figure 1 in reference.[16] Off-resonance effects are calculated by defining an off-resonance vector $\Im$ that extends in and beyond the bandwidth of the pulses. The magnetization $\mathbf{M_P}$ in Appendix C after the soft excitation 90° pulse vs $\Im$ is calculated as explained in Figures 4 and 5 in reference.[16] The α and β parameters of the RF pulses vs $\Im$ are calculated from the b_1 waveform with Equations (1-4) and Figure 1 in reference.[16] These α, β become 2-dimensional matrices that depend on off-resonance $\Im$ and the RF pulse number n, rather than vectors with N components. They are used

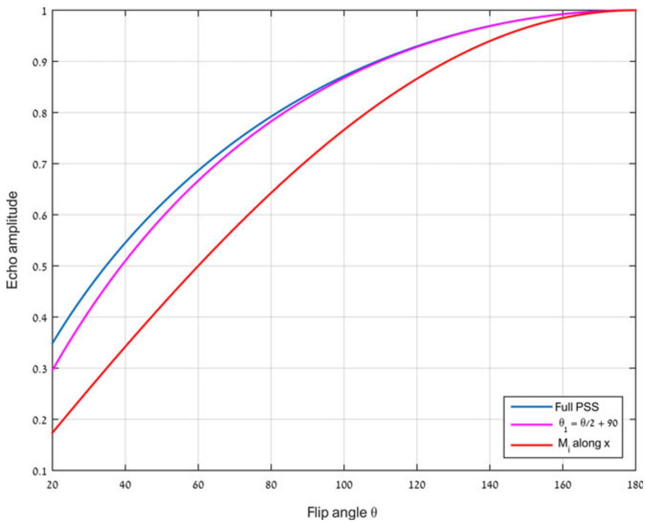

FIGURE 3 Comparison between the pseudo steady-state (PSS) signal vs flip angle θ (neglecting relaxation) for (i) Equation (19b) where $\mathbf{M_i}$ is along *x*, (ii) Equation (24b) with θ_1=θ/2 + 90°, and (iii) Equation (27) with $\mathbf{M_A} = \mathbf{M_{Amax}}$

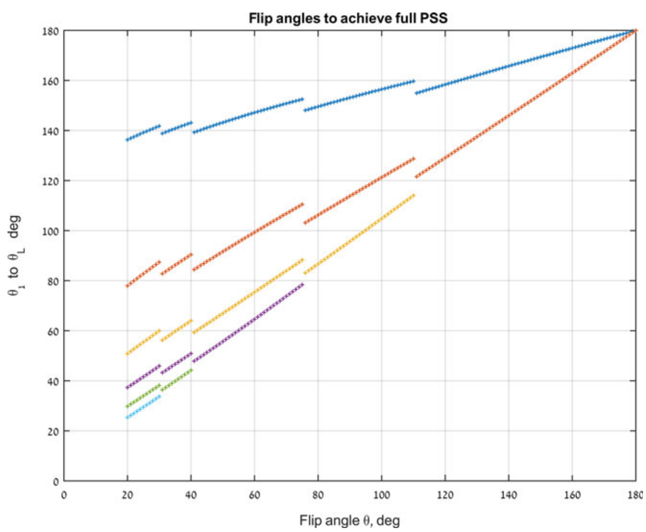

FIGURE 4 Optimized flip angles θ_1 to θ_L vs θ, the flip angle of the train. θ_1-θ_L for each given θ are marked by crosses at the intersections with the vertical θ line. Note the increase of *L* when θ decreases

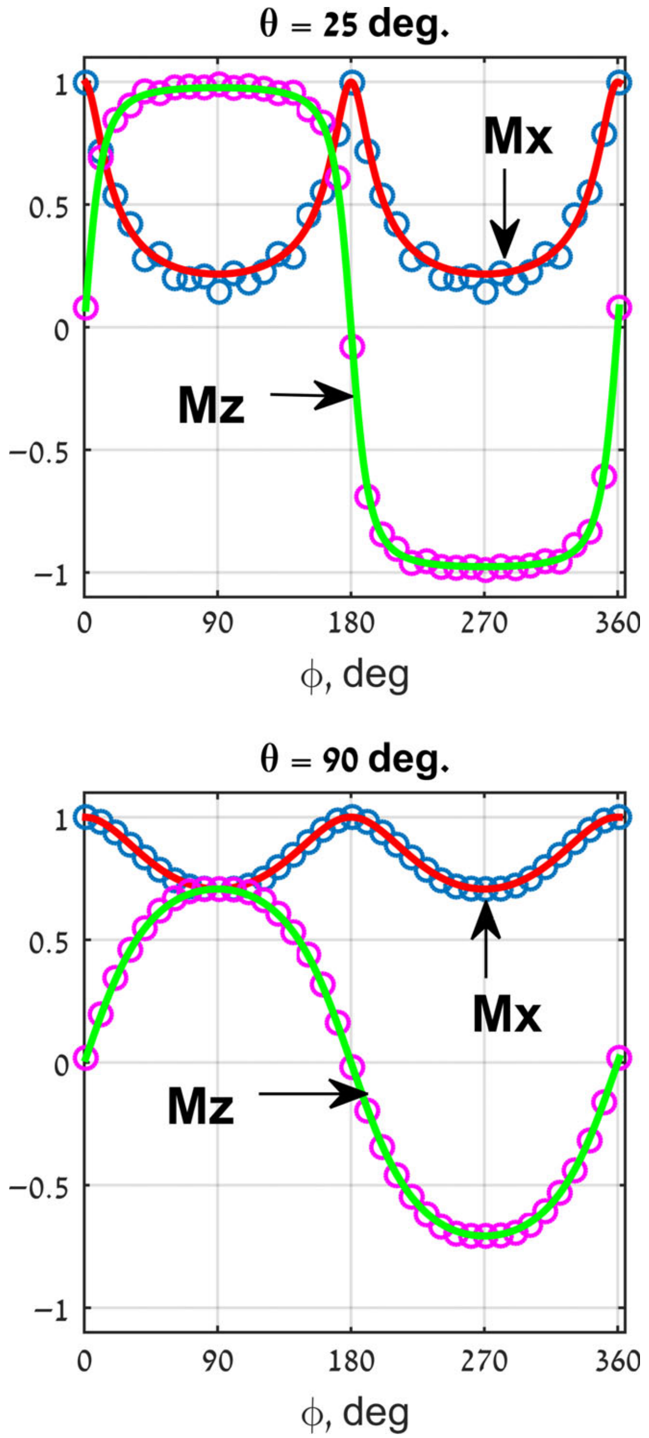

FIGURE 5 Comparison between M_x (ϕ) and M_z (ϕ) after the first *L* pulses with flip angles from Figure 4, with the theoretical $\mathbf{M_{Amax}}$ in (11b) vs ϕ. The calculated M_x and M_z are plotted as blue and magenta circles, respectively. The theoretical M_x and M_z from (11b) are plotted as full red and full green lines, respectively. The flip angles θ used are 25° (top Figure) and 90° (bottom Figure)

exactly as in Appendix C to calculate the signal amplitude vs $\Im$ (slice profile). The overall echo amplitude is the sum of the signal over all the excited off-resonance values $\Im$.

3 | IMPLEMENTATION FOR SEQUENCES WITH A GIVEN $\mathbf{M_I}$

In this section, we apply the vector model from the previous section and calculate the magnetization and echo for sequences with a given initial magnetization $\mathbf{M_i}$ and *N* periodic operators. We neglect relaxation and assume a constant flip angle, so the analytic solution of Appendix A can be used to find $\mathbf{M^{(n)}}$ and echo signal for $n = 1$ to *N*.

As shown in (A5), $\mathbf{M^{(n)}}$ consists of a pseudo steady-state term $\mathbf{M_A}$ and an oscillatory term $\mathbf{M_P^{(n)}}$. Since only $\mathbf{M_A}$ gives a useful signal, it is useful to calculate the Fourier coefficients of $\mathbf{M_A}$ using (15) and (16):

$$\mathcal{A}_k^{(n)} = \frac{1}{2\pi}\int_{-\pi}^{\pi} M_{A,xy}^{(n)}(\phi)\, e^{-i\phi k}\, d\phi; \quad \mathcal{B}_k^{(n)} = \frac{1}{2\pi}\int_{-\pi}^{\pi} M_{A,z}^{(n)}(\phi)\, e^{-i\phi k}\, d\phi \tag{17a}$$

where $M_{A,xy}^{(n)}$ and $M_{A,z}^{(n)}$ in (17a) are the x-y and z magnetization of $\mathbf{M_A}$ after the nth RF pulse. Since the echo signal is the zero Fourier coefficient $A_0^{(n)}$ of $\mathbf{M^{(n)}}$ (Equation (15b)) and $\mathbf{M^{(n)}} = \mathbf{M_A} + \mathbf{M_P^{(n)}}$ (Equation (A5)):

$$\text{Echo}(n) = \frac{1}{2\pi}\int_{-\pi}^{\pi} M_{xy}^{(n)}(\phi)\, d\phi = \mathcal{A}_0^{(n)} + \frac{1}{2\pi}\int_{-\pi}^{\pi} \mathbf{M}_{P,xy}^{(n)}(\phi)\, d\phi \equiv \mathcal{A}_0 + \mathbf{I^{(n)}} \tag{17b}$$

where $\boldsymbol{M_{P,xy}^{(n)}}$ is the x-y component of $\mathbf{M_P^{(n)}}$. The integral $\boldsymbol{I^{(n)}} = \frac{1}{2\pi}\int_{-\pi}^{\pi} \boldsymbol{M}_{P,xy}^{(n)}(\phi) d\phi$ in (17b) is calculated by computing $\mathbf{M_P^{(n)}}$ using $\mathbf{R^{(n)}}$ in (A2) and integrating over ϕ as shown below. The echo is a sum of a constant term $\mathcal{A}_0$ and a n-dependent term $\boldsymbol{I^{(n)}}$.

3.1 | $\mathbf{M_i}$ along the x-axis

$\mathbf{R_{prep}}$ is a 90° RF pulse in $-y$, so $\mathbf{M_i}$ is along the x-axis as in a standard RARE sequence. From (10), the pseudo steady-state magnetization $\mathbf{M_A}$ is

$$M_{Ax} = \frac{1}{1+\lambda^2}; \qquad M_{Ay} = 0; \qquad M_{Az} = \frac{\lambda}{1+\lambda^2}. \tag{18a}$$

The perpendicular rotating component $\mathbf{M_P}$ is:

$$M_{Px} = \frac{\lambda^2}{1+\lambda^2}; \qquad M_{Py} = 0; \qquad M_{Pz} = \frac{-\lambda}{1+\lambda^2} \tag{18b}$$

M_{Ax} is both symmetric and pi-symmetric in ϕ. Using Appendix B and Equation (17a), the Fourier coefficients of $\mathbf{M_A}$ in Equation (18a) are:

$$\mathcal{A}_{2n} = \mathcal{A}_{-2n} = \frac{1}{\pi}\int_0^{\pi} \frac{\cos(2nx)}{1+\lambda^2} dx \quad \text{where } n = 0,\ 1,\ 2,\ \ldots. \tag{19a}$$

Using the online integration calculator[20], we find that

$$\mathcal{A}_0 = \frac{1}{\sqrt{\frac{C^2}{S^2}+1}} = S; \quad \mathcal{A}_2 = \mathcal{A}_{-2} = \frac{S + S^3 - 2S^2}{C^2}. \tag{19b}$$

M_{Az} in (18a) is antisymmetric and pi-antisymmetric in ϕ. Therefore, the Fourier coefficients of M_{Az} are:

$$\mathcal{B}_n = -\mathcal{B}_{-n} = \frac{-i}{\pi}\int_0^{\pi} \frac{\lambda \cdot \sin(nx)}{1+\lambda^2} dx \qquad n = 1,\ 3,\ 5,\ \ldots. \tag{19c}$$

Using an integration calculator[20]

$$\mathcal{B}_1 = -\mathcal{B}_{-1} = -i\frac{S - S^2}{C}. \tag{19d}$$

$\mathcal{A}_0$ in (19b) was originally obtained by Alsop.[13]

The integral $\boldsymbol{I^{(n)}}$ for $\mathbf{M_i}$ in x and phase error ξ is calculated by Equations (31-35) below. Therefore, the echo here is equal to Equation (34) with $\xi = 0$, and $\boldsymbol{I^{(n)}}$ is equal to I_1 in Equation (35a) and Figure 8. From (17b):

$$\text{Echo}(n) = \mathcal{A}_0 + \boldsymbol{I^{(n)}} = \mathcal{A}_0 + I_1 = S + \frac{1}{\pi}\int_0^{\pi} \frac{\lambda^2}{1+\lambda^2} \cdot \exp(in\psi) d\phi \tag{20}$$

where $\exp(in\ \psi)$ in (20) is given by Equation (9b).

Lukzen et al[14,15] provides an analytic approximation that converges to the exact solution (20) for n $\gtrsim$ 8.

3.2 | Multi-echo sequence with a different first flip angle

Hennig and Scheffler[21] showed that using a larger first flip angle $\theta_1 = 90° + \theta/2$ it is possible to increase the signal of the pseudo steady-state echo $\mathcal{A}_0$. We shall analyze this and provide analytic expressions.

The prep operator is the 90°_{-y} excitation followed by the first periodic operator with flip angle θ_1. $\mathbf{M_i}$ is the magnetization at the beginning of the second periodic operator. Using (2) and (5)

$$M_{ix} = 1 - 2C_0^2 \cdot \sin^2(\phi); \quad M_{iy} = -2C_0^2 \cdot \sin(\phi)\cos(\phi); \quad M_{iz} = 2C_0S_0 \cdot \sin(\phi). \tag{21}$$

Where $C_0 \equiv \cos\left(\frac{\theta_1}{2}\right)$ and $S_0 \equiv \sin\left(\frac{\theta_1}{2}\right)$. $\mathbf{M_A}$ is computed by substitution of (21) into Equation (10):

$$M_{Ax} = \frac{1 - 2C_0^2\sin^2(\phi) + 2C_0S_0\sin^2(\phi) \cdot \frac{C}{S}}{1 + \frac{C^2}{S^2}\sin^2(\phi)}; \quad M_{Az} = \frac{C}{S}\sin(\phi) \cdot M_{Ax} \tag{22}$$

where M_{Ax} and M_{Az} are the x and z components of $\mathbf{M_A}$. To find θ_1 that maximizes M_{Ax}, we calculate $\frac{dM_{Ax}}{d\theta_1} = 0$. The result is

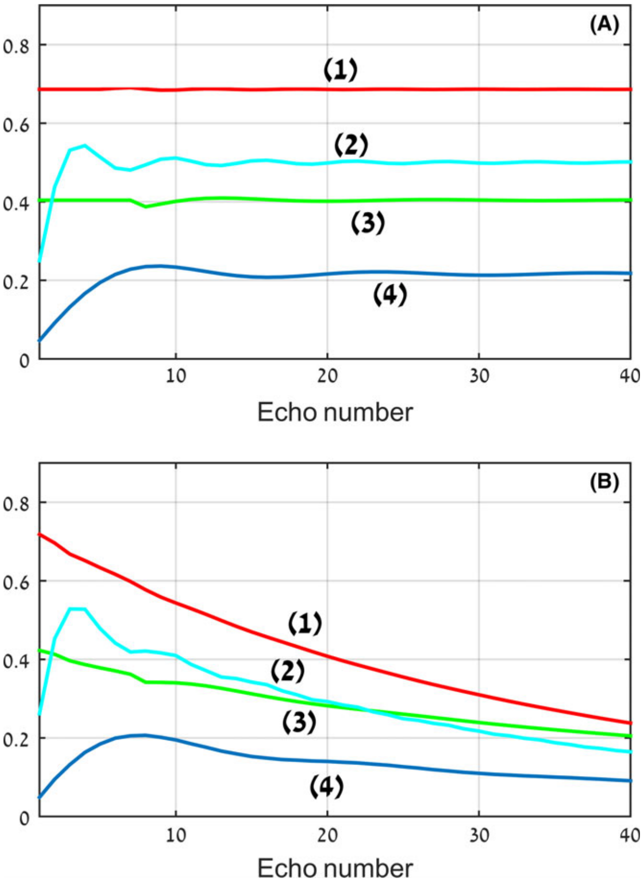

FIGURE 6 A, Comparison between optimized RARE sequences (the first L flip angles are taken from Figure 4 and Table 1 and the first L echoes are divided by $R(m)$ in Equation (30)) to constant flip sequences. The RF pulses are non-selective and $T_1 = T_2 = \infty$. (1) Optimized with $\theta = 60°$. (2) Constant flip with $\theta = 60°$. (3) Optimized with $\theta = 25°$. (4) Constant flip. $\theta = 25°$. B, Comparison between optimized RARE sequences (flip angles and echo compensation) to constant flip sequences for $T_1/T_2 = 1000/100$ ms with echo spacing of 5 ms. The RF pulses are slice-selective SLR linear phase. (1) Optimized with $\theta = 60°$. (2) Constant flip with $\theta = 60°$. (3) Optimized. $\theta = 25°$. (4) Constant flip. $\theta = 25°$

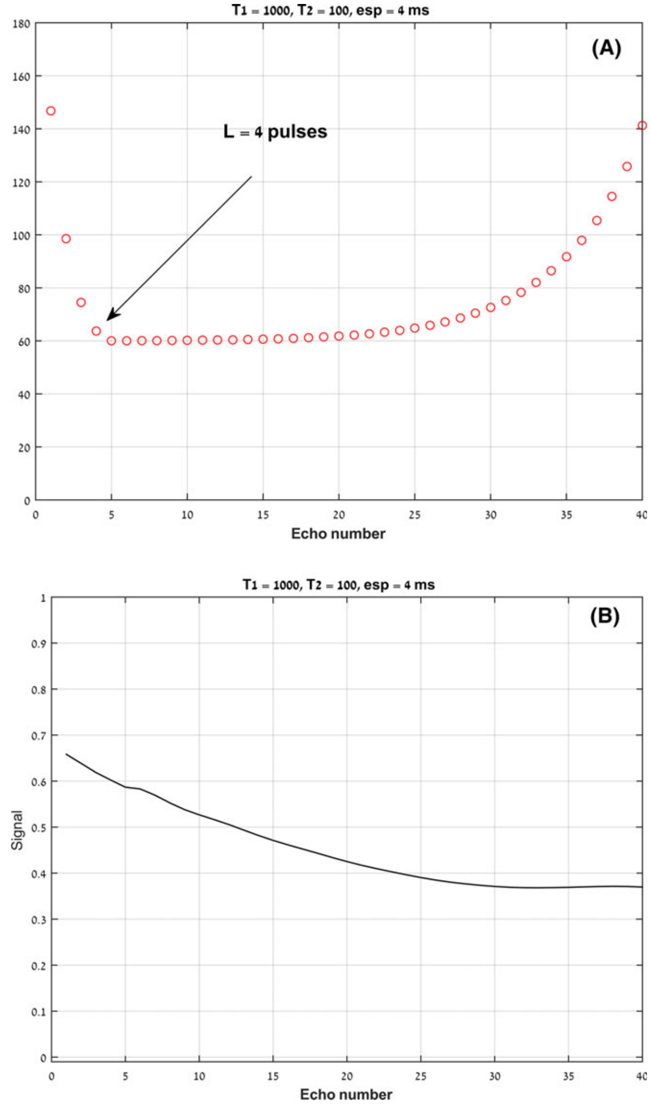

FIGURE 7 A, RF flip angles of a train with 40 pulses and echo spacing of 5 ms. The first $L = 4$ pulses sets the magnetization to $\mathbf{M_{Amax}}$ for $\theta = 60°$. Increasing the flip angles to 140° toward the end reduces signal decay and image blurring. B, Signal with T_1/T_2 of 1000/100 ms and echo space of 5 ms with flip angles from Figure 7A. The signal with constant flip angle of 60° is shown in Figure 6B at graph (1). The signal in this Figure decays less than in Figure 6B graph (1)

$$\cos(\theta_1)\cdot\frac{C}{S} = -\sin(\theta_1) \quad => \quad \theta_1 = \frac{\theta}{2} + 90°. \tag{23}$$

The optimal first flip angle that maximizes $\mathbf{M_A}$ is independent of ϕ and depends only on θ. Since M_{Ax} is symmetric and pi-symmetric and M_{Az} is antisymmetric and pi-antisymmetric, its Fourier coefficients are given by Equations (19a) and (19c) with M_{Ax} and M_{Az} in (18) replaced by (22). Using integral calculator[20], we find:

$$\mathcal{A}_0 = S + \left(2C_0S_0\frac{C}{S} - 2C_0^2\right)\cdot\frac{S^2 - S^3}{C^2}. \tag{24a}$$

If $\theta_1 = \frac{\theta}{2} + 90°$, Equation (24a) simplifies to

$$\mathcal{A}_0 = S + \frac{S\cdot(1-S)}{1+S} \tag{24b}$$

$\mathcal{A}_0$ in (24b) is larger by $S(1-S)/(1+S)$ from (19b).

The first echo of this sequence is acquired at the end of the first periodic operator with flip angle θ_1, where the magnetization is $\mathbf{M_i}$ (Equation (21)) and the echo amplitude is:

$$\begin{aligned} \text{echo } 1 &= \frac{1}{2\pi}\int_{-\pi}^{\pi}(M_{ix} + iM_{iy})d\phi \\ &= 1 - \frac{2C_0^2}{2\pi}\int_{-\pi}^{\pi}\sin^2(\phi)d\phi \\ &= 1 - C_0^2 = S_0^2. \end{aligned} \tag{25}$$

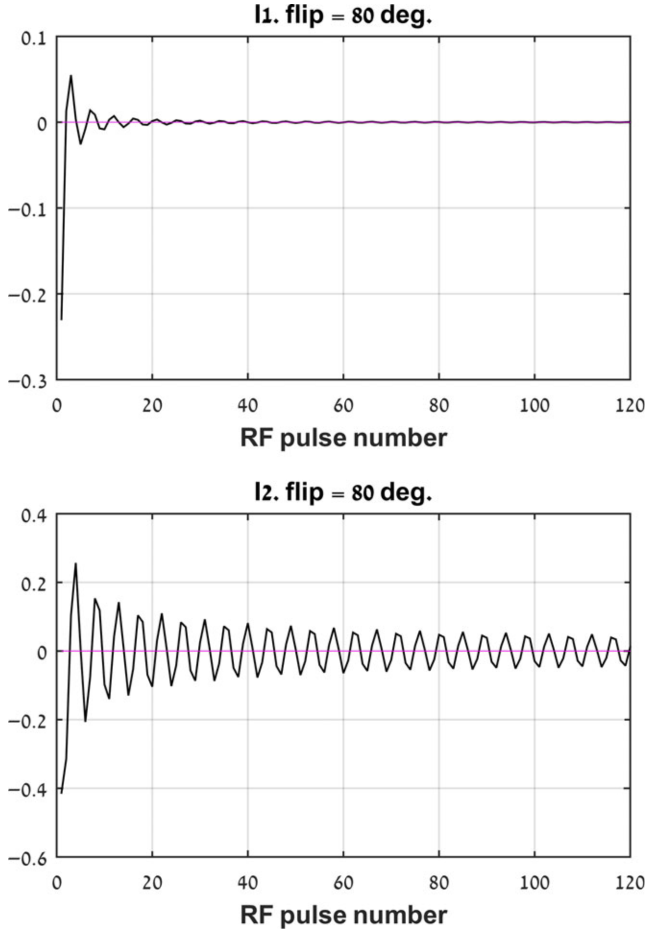

FIGURE 8 The integral I_1 (Equation (35a); top Figure) and I_2 (Equation (35b); bottom Figure) for n = 1-120 RF pulses. Flip angle = 80°

The amplitudes of the echoes from the second to the last are given by (17b):

$$\mathrm{Echo}(n) = \mathcal{A}_0 + \boldsymbol{I}^{(\boldsymbol{n})}. \tag{26}$$

$\mathbf{I}^{(\mathbf{n})}$ is calculated in Appendix D using the matrix $\mathbf{R}^{(\mathbf{n})}$ in Equation (A2). It is a sum of 2 integrals in Equation (D6). These integrals do not have an analytic solution, but can be easily calculated by numerical integration. Note that the echo with $n = 1$ in (26) is the second acquired echo, and the amplitude of the first echo is given by (25). The echo amplitudes of the Hennig-Scheffler sequence for θ = 90° and 120° are plotted in Figure 5 in reference.[21]

3.3 | Multi-echo sequence with optimized initial magnetization $\mathbf{M_i}$

To maximize $\mathbf{M_A}$ and minimize $\mathbf{M_P}$, we must align the initial magnetization $\mathbf{M_i}$ as close as possible to $\mathbf{V_A}$. If $\mathbf{M_i}$ and $\mathbf{V_A}$ are aligned for all ϕ, maximum pseudo steady-state $\mathbf{M_{Amax}}$ (Equation (11b)) is obtained, and the echo signal is

$$E_{\mathrm{PSS}} = \frac{1}{2\pi}\int_{-\pi}^{\pi}\frac{d\phi}{\sqrt{1+\lambda^2}} = \frac{1}{\pi}\int_{0}^{\pi}\frac{d\phi}{\sqrt{1+\lambda^2}}. \tag{27}$$

A similar result is given by Alsop (see Figure 1 and equation (8) in reference (13)). This integral can be easily evaluated numerically, but has no simple analytic solution. E_{PSS} in (27) is the highest possible signal for a given θ as shown by Figure 3, which compares the pseudo steady-state echo signal of Equation (19b), where $\mathbf{M_i}$ is along x, Equation (24b) with $\theta_1 = \frac{\theta}{2} + 90°$ and Equation (27) with maximum pseudo steady-state $\mathbf{M_{Amax}}$ vs θ.

To align $\mathbf{M_i}$ with $\mathbf{V_A}$ for all ϕ, we vary the flip angles θ_1 to θ_L of the first L RF pulses, such that $\mathbf{R_{prep}}$ consists of L RF pulses. The 2 × 2 unitary matrix of $\mathbf{R_{prep}}$ is:

$$\mathbf{R_{prep}} = \prod_{k=1}^{L}\begin{pmatrix} C_k z & iS_k \\ iS_k & C_k z^{-1}\end{pmatrix}\cdot R(-90)_y. \tag{28}$$

Where S_k, C_k is $\sin(\theta_k/2)$ and $\cos(\theta_k/2)$, respectively, k = 1-L. $\boldsymbol{M_i} = \left[M_{ix},\ M_{iy},\ M_{iz}\right]^T$ is calculated from R_{prep} using (5) and $R_{MA} = \frac{|\boldsymbol{M}_A|}{|\boldsymbol{M}_{\mathrm{Amax}}|}$ is computed using (11c). The optimal flip angles θ_1 to θ_L are obtained when R_{MA} is as close as possible to 1. Since R_{MA} depends on ϕ, the optimization minimizes

$$\delta \equiv 1 - \frac{1}{2\pi}\int_{-\pi}^{\pi} R_{MA}(\phi)\, d\phi. \tag{29}$$

$\delta \approx 0$ implies that $\mathbf{M_i}$ is aligned with $\mathbf{V_A}$ and $\mathbf{M_P}$ is close to zero for all ϕ. θ_1 to θ_L that minimize δ are computed with the Nelder-Mead minimization algorithm (MATLAB "fminsearch" and reference (22)). For all flip angles 180° ≥ θ ≥ 20°, the minimization converges within a few iterations. The number L of pulses required to reduce δ below a given threshold vary with flip angle, where for large flip angles (θ ≥ 110°) L = 2 pulses and for low flip angles (θ ≤ 25°) L = 6. The minimization of δ is carried out for each θ, and a table of optimal flip angles vs θ is created. The (arbitrary) threshold of δ is set to 1%, ie, δ ≤ 0.01 for all θ. We have segmented the flip angles into 5 segments with different L in each segment. Table 1 lists the flip angles range, L and maximum δ, referred to as δmax, in each segment. $\delta_{\max}$ and L are larger for lower flip angles. The small $\delta_{\max}$ in the table indicates that R_{MA} is close to 1 and maximum pseudo steady-state is obtained for all ϕ and θ. The table of optimized flip angles θ_1 to θ_L vs θ is shown in Figure 4. This table needs to be calculated only once. For any user-selected θ, the optimal set of flip angles is picked from the table.

To verify that $M_x(\phi)$ and $M_z(\phi)$ after the first L pulses are fully aligned with $\mathbf{M_{Amax}}$, we calculated $M_x(\phi)$ and $M_z(\phi)$ for all θ and ϕ after L pulses using the flip angles θ_1 to θ_L from Figure 4, and compared them to the theoretical

TABLE 1 Flip angle ranges, number of pulses L, and maximum δ in each segment

Segment	Range of flip angles (degrees) in each segment	Number of pulses, L	δ_{max}
1	20-30	6	0.0036
2	31-40	5	0.0020
3	41-75	4	0.0006
4	76-110	3	2.5×10^{-4}
5	111-180	2	1.1×10^{-4}

result in Equation (11b). The comparison showed very good agreement for all ϕ and θ. Figure 5 shows calculated $M_x(\phi)$ and $M_z(\phi)$ for ϕ = 0°-360° and flip angles θ = 25° and 90° together with the theoretical $\mathbf{M_{Amax}}$ in Equation (11b).

Figure 4 shows that θ_1 to θ_L are much higher than the corresponding flip angle θ of the pulse train. Therefore, echoes 1 to L are much higher than echo L + 1 to the end of the train, and must be compensated to ensure equal amplitudes for all echoes from 1 to the end of the train. This is done by calculating the ratio $R(m)$ between echo m (m = 1-L) to E_{PSS}, because the amplitude of the echoes from L + 1 to the end is E_{PSS}.

$$R(m) = \frac{E(m)}{E_{\mathrm{PSS}}}. \tag{30}$$

$E(m)$ is the amplitude of echo m

$$E(m) = \frac{1}{2\pi}\int_{-\pi}^{\pi} M_{xy}^{(m)}(\phi)\, d\phi$$

$M_{xy}^{(m)}(\phi)$ is calculated from its Cayley-Klein parameters and Equation (5).

$R(m)$ vs θ is computed by Equation (30) and stored in a table (not shown). When the user selects θ, echoes 1 to L are compensated by dividing the k-space data of the first L echoes by $R(m)$ (m = 1-L) during reconstruction.

Figure 6A compares echo amplitudes with θ_1 to θ_L optimization and $R(m)$ compensation, to echo amplitudes acquired with constant flip angles and $\mathbf{M_i}$ along x. All echoes were calculated with Equation (16c). Graphs (1) and (3) show the optimized and compensated echoes for flip angles θ = 25° and 60°. Graphs (2) and (4) show the constant flip angles echoes for θ = 25° and 60°. The RF pulses in Figure 6A are non-selective and relaxation is ignored. The echoes in graphs (1) and (3) are stable from echo 1, which enables scanning tissues with short T_2. As expected, the echo amplitudes in graphs (1) and (3), where $\mathbf{M_i} \approx \mathbf{M_A}$, are higher than in graphs (2) and (4).

The above θ_1 to θ_L optimization and echo compensation neglects relaxation and assumes that the RF pulses are non-selective. To examine the validity of the results in a more realistic sequence, we simulated the sequence in Figure 1 with T_1 = 1000 ms, T_2 = 100 ms and selective RF pulses. The excitation and refocusing pulses were linear phase Shinnar-Le Roux (SLR)[16] pulses with bandwidth of 1 kHz and 1.9 kHz, respectively, and echo spacing of 5 ms. The off-resonance vector $\mathfrak{I}$ had 160 points from −1.5 kHz to 1.5 kHz. Echo amplitudes are shown in Figure 6B for flip angles θ = 60° and 25°. Graphs (1) and (3) show optimized and compensated echo amplitudes with θ_1 to θ_L taken from Figure 4 and echo compensation ratios $R(m)$ taken from the table that we used in Figure 6A. Graphs (2) and (4) in Figure 6B show echo amplitudes with constant flip angles of θ = 25° and 60°. The echoes in graphs (1) and (3) decay smoothly from echo 1 due to relaxation, and have higher amplitudes than the echoes in graphs (2) and (4). These results show that the θ_1 to θ_L flip angle optimization and echo compensation can be used successfully with slice-selective pulses and finite relaxation times.

3.4 | RF flip angles optimization from θ_L to the end of the echo train

As shown in the previous section, maximum pseudo steady-state magnetization M_{Amax} is achieved after L RF pulses for any θ, and $\mathbf{M_i}$ is aligned with $\mathbf{V_A}$. For low θ, the z component of $\mathbf{M_{Amax}}$ is larger and the x component (and the signal) is smaller. For larger θ, the z component decreases and the x component increases. This is evident from Figure 3 where the echo signal increases with flip angle. We can use this to our advantage, by setting the first L pulses to $\mathbf{M_{Amax}}$ with a low flip angle, and then increase θ gradually toward the end of the echo train, while increasing the signal. In the absence of relaxation, if $\mathbf{M_i}$ is aligned with $\mathbf{V_A}$ and the flip angle gradually increases, the magnetization M follows $\mathbf{V_A}$.[8] As θ increases, $\mathbf{V_A}$ and M remain aligned, and rotate toward the x-axis and the signal increases. If relaxation is present, the decay of the signal along the echo train due to relaxation becomes more moderate if θ increases. This is very useful because signal decay along the train broadens the point spread function which causes image blurring. Therefore, increasing the flip angle reduces image blurring.

Figure 6B shows that if the flip angle θ after the first L RF pulse is retained, there is significant signal decay along the train due to relaxation. To minimize signal decay, the flip angle gradually increases to maximize the signal toward the end of the train. Figure 7A shows the flip angles for a train with 40 pulses and echo space of 5 ms. After L = 4 pulses, $\mathbf{M_{Amax}}$ with flip angle θ = 60° is achieved. In later RF pulses, θ increases exponentially toward 140°. The echo amplitude for a sample with T_1 = 1000 ms and T_2 = 100 ms is shown in Figure 7B.

The signal decay is much more moderate compared to the decay with a constant flip of 60° shown in Figure 6B graph (1). In general, the optimal flip angles to use depend on relaxation times, echo train length (ETL), the amount of signal decay that one can tolerate and the location in the train of the echo at the k-space center. Since an acceptable signal decay is subjective and depends on many parameters, there is no unique optimal set of flip angles. Optimization methods for different applications are found in references.[8,23,24]

4 | ANALYSIS AND CORRECTION OF PHASE ERRORS

In this section, we shall calculate the signals in case the initial magnetization $\mathbf{M_i}$, which is assumed to be on the x-axis, is phase-shifted from the x-axis toward the y-axis by system imperfections, and then show how to correct it. Phase shifts of $\mathbf{M_i}$ toward the y-axis are caused by eddy currents and/or inaccurate gradient pulses. They increase significantly at off-center locations[25] or after strong gradient pulses in diffusion weighted sequences.[26] To simplify the analysis, we ignore relaxation and assume a constant flip angle.

$\mathbf{M_A}$ is in the x-z plane, so the y component of $\mathbf{M_i}$ is perpendicular to $\mathbf{M_A}$ and oscillates in a plane perpendicular to $\mathbf{M_A}$, which causes artifacts. Suppose the initial magnetization $\mathbf{M_i}$ after the 90°_{-y} excitation pulse is phase-shifted due to system imperfections by ξ radians:

$$\mathbf{M_i} = M_i(\cos\xi \cdot \hat{x} + \sin\xi \cdot \hat{y}).$$

Where $\hat{x}$ and $\hat{y}$ are unit vectors along x and y. For long TR scans, $M_i = M_0 = 1$. We substitute $\mathbf{M_i}$ into Equation (10), to find the rotating magnetization $\mathbf{M_p}$:

$$M_{px} = \frac{\lambda^2}{1+\lambda^2} M_{ix};\;\; M_{py} = M_{iy};\;\; M_{pz} = \frac{-\lambda}{1+\lambda^2} M_{ix} \quad (31a)$$

where $M_{ix} = M_i \cos\xi$ and $M_{iy} = M_i \sin\xi$.

The pseudo steady-state magnetization $\mathbf{M_A}$ is

$$M_{Ax} = \frac{M_i \cos\xi}{1+\lambda^2};\quad M_{Az} = \lambda\, M_{Ax} \quad (31b)$$

The magnetization $\mathbf{M^{(n)}}$ after n RF pulses is calculated with the matrix $\mathbf{R^{(n)}}$ in (A2). $\mathbf{M_A}$ is not affected by $\mathbf{R^{(n)}}$, and $\mathbf{M_P^{(n)}}$ in Equation (A5) is obtained by multiplying $\mathbf{R^{(n)}}$ by $\boldsymbol{M_P} = \left[M_{px},\, M_{py},\, M_{pz}\right]^T$. The echo is computed by integrating $M^{(n)} = M_A + M_P^{(n)}$ over ϕ from $-\pi$ to π. From (A2) and (31), we calculate the contribution of $\mathbf{M_P}$ to the echo:

$$\mathrm{Re(echo)}_{MP} = \frac{1}{2\pi}\int_{-\pi}^{\pi}\left[\left(c_1c_2^2+s_2^2\right)\cdot M_{px} + c_2s_2(1-c_1)\cdot M_{pz}\right]d\phi + \frac{M_{iy}}{2\pi}\cdot\int_{-\pi}^{\pi} c_2s_1 d\phi \quad (32a)$$

$$\mathrm{Im(echo)}_{MP} = -\frac{1}{2\pi}\int_{-\pi}^{\pi} c_2s_1\cdot M_{px}d\phi + \frac{1}{2\pi}\int_{-\pi}^{\pi} s_1s_2\cdot M_{pz}d\phi + \frac{M_{iy}}{2\pi}\cdot\int_{-\pi}^{\pi} c_1 d\phi. \quad (32b)$$

$s_2 = \sin(\delta_1)$ and $c_2 = \cos(\delta_1)$ are given by (A1a) and (A1b); $c_1 = \cos(n\psi)$ and $s_1 = \sin(n\psi)$ are given by (A3). The right term of (32a) vanishes because ψ and s_1 is symmetric in ϕ (Equation (9)) and c_2 is antisymmetric (Equation (A1b)). The left term in (32b) vanishes because c_2s_1 is antisymmetric in ϕ and M_{px} is symmetric (Equation (31a)). The middle term in (32b) vanishes because s_1s_2 is symmetric and M_{pz} antisymmetric. The right term in (32b) is nonzero because c_1 is symmetric in ϕ. The full echo is obtained by adding the integral over ϕ of M_A (Equation (31b)) to Equation (32). Assuming $M_i = 1$:

$$\mathrm{Re(echo)}_{MA} = \frac{1}{2\pi}\int_{-\pi}^{\pi} M_{Ax}d\phi = \frac{1}{2\pi}\int_{-\pi}^{\pi}\frac{\cos\xi}{1+\lambda^2}d\phi = S\cdot\cos\xi. \quad (33)$$

The final echo is a sum of (32) and (33):

$$\mathrm{Echo} = (I_1 + S)\cdot\cos\xi + iI_2\cdot sin\xi \quad (34)$$

where I_1 is given by:

$$I_1 = \frac{1}{2\pi}\int_{-\pi}^{\pi}\left[\left(c_1c_2^2+s_2^2\right)\cdot\frac{\lambda^2}{1+\lambda^2} - c_2s_2(1-c_1)\cdot\frac{\lambda}{1+\lambda^2}\right]d\phi$$

and I_2 is

$$I_2 = \frac{1}{2\pi}\cdot\int_{-\pi}^{\pi} c_1 d\phi$$

substituting $s_2 = \sin(\delta_1) = \frac{1}{\sqrt{1+\lambda^2}}$, and $c_2 = \cos(\delta_1) = \frac{\lambda}{\sqrt{1+\lambda^2}}$ into I_1:

$$I_1 = \frac{1}{2\pi}\int_{-\pi}^{\pi}\frac{\lambda^2}{1+\lambda^2}\cdot\cos(n\psi)\,d\phi = \frac{1}{\pi}\int_{0}^{\pi}\frac{\lambda^2}{1+\lambda^2}\cdot\exp(in\psi)\,d\phi \quad (35a)$$

$$I_2 = \frac{1}{2\pi}\int_{-\pi}^{\pi} c_1 d\phi = \frac{1}{2\pi}\int_{-\pi}^{\pi}\cos(n\psi)\,d\phi = \frac{1}{\pi}\int_{0}^{\pi}\exp(in\psi)\,d\phi. \quad (35b)$$

Both I_1 and I_2 have no simple analytic expression, but can be easily evaluated numerically. Figure 8 shows I_1 and I_2 for n = 1-120 RF pulses and flip angle θ = 80°. As expected I_1 oscillates, but decays to zero after a few pulses, while I_2 oscillations persist even after 120 pulses. Equation

(35) shows that the oscillations of I_1 are caused by the rotation of M_{px} in (31a) by $n\psi$ radians, and the oscillations of I_2 are caused by the rotation of $M_{py} = M_{iy}$ in (31a) by $n\psi$ radians.

In summary, the phase error ξ generates artifacts because (i) the imaginary part of the echo in (34) is oscillatory and (ii) the real part of the echo ("good" signal) amplitude decreases by cosξ. To eliminate the oscillatory part one can null the imaginary part of the echo, but this cannot be done in practice due to an unknown instrumentation-dependent receiver phase.

To recover the original signal S, we use another excitation where the phase of the excitation RF pulse is shifted by 90° such that $\xi \rightarrow \xi + 90°$. The echo signals E_1 and E_2 from these 2 excitations are given by

$$\begin{aligned} E_1 &= (I_1 + S) \cdot \cos\xi + iI_2 \cdot sin\xi; \\ E_2 &= -(I_1 + S) \cdot sin\xi + iI_2 \cos\xi. \end{aligned} \tag{36}$$

E_1 and E_2 are combined by adding and subtracting E_1 and $-i\mathrm{E}_2$ to yield the even and odd echoes E_{even} and E_{odd}[9]:

$$\begin{aligned} E_{\text{even}} &= \frac{E_1 + (-iE_2)}{2} = \frac{I_1 + S + I_2}{2}\exp(i\xi); \\ E_{\text{odd}} &= \frac{E_1 - (-iE_2)}{2} = \frac{I_1 + S - I_2}{2}\exp(-i\xi). \end{aligned} \tag{37}$$

The phase difference 2ξ between E_{even} and E_{odd} is used to recover the signal $S = \sin(\theta/2)$ and eliminate I_2:

$$I_1 + S = | E_{\text{even}} + \exp(i2\xi) \cdot E_{\text{odd}} | \tag{38}$$

The full reconstruction algorithm is described in,[25] where the phase 2ξ is derived from a low resolution version of E_{even} and E_{odd}. The phases of the RF pulses in the 2 excitations are not unique,[9] but Equation (36) is the simplest to implement.

REFERENCES

1. Hennig J, Nauerth A, Friedburg H. RARE imaging: a fast imaging method for clinical MR. *Magn Reson Med*. 1986;3:823-833.
2. Woessner DE. Effects of diffusion in nuclear magnetic resonance spin-echo experiments. *J Chem Phys*. 1961;34:2057-2061.
3. Hennig J. Multiecho imaging sequences with low refocusing flip angles. *J Magn Reson*. 1988;78:397-407.
4. Hennig J. Echoes – how to generate, recognize use or avoid them in MR imaging sequences. *Concepts Magn Reson*. 1991;3:125-143.
5. Hennig J, Weigel M, Scheffler K. Calculation of flip angles for echo trains with predefined amplitudes with the extended phase graph (EPG) algorithm: principles and applications to Hyperechoes and Traps sequences. *Magn Reson Med*. 2004;51:68-80.
6. Weigel M. Extended phase graphs: dephasing, RF pulses, and echoes - pure and simple. *J Magn Reson Imaging*. 2015;41:266-295.
7. Zur Y. Algorithm to calculate the NMR signal of a multi spin-echo sequence with relaxation and spin-diffusion. *J Magn Reson*. 2004;171:97-106.
8. Hennig J, Weigel M, Scheffler K. Multi-echo sequences with variable refocusing flip angles: optimization of signal behavior using smooth transitions between pseudo steady states (TRAPS). *Magn Reson Med*. 2003;49:527-535.
9. Zur Y, Stokar S. A phase-cycling technique for canceling spurious echoes in NMR Imaging. *J Magn Reson*. 1987;71:212-228.
10. Le Roux P, Hinks RS. Stabilization of Echo Amplitudes in FSE Sequences. *Magn Reson Med*. 1993;30:183-191.
11. Carr HY, Purcell EM. Effects of diffusion on free precession in nuclear magnetic resonance experiments. *Phys Rev*. 1954;94:630.
12. Meiboom S, Gill D. Modified spin-echo method for measuring nuclear relaxation times. *Rev Sci Inst*. 1958;29:688-691.
13. Alsop DC. The sensitivity of low flip angle RARE imaging. *Magn Reson Med*. 1997;37:176-184.
14. Lukzen NN, Savelov AA. Analytical derivation of multiple spin echo amplitudes with arbitrary refocusing angle. *J Magn Reson*. 2007;185:71-76.
15. Lukzen NN, Petrova MV, Koptyug IV, Savelov AA, Sagdeev RZ. The generating functions formalism for the analysis of spin response to the periodic trains of RF pulses. Echo sequences with arbitrary refocusing angles and resonance offsets. *J Magn Reson*. 2009;196:164-169.
16. Pauly J, Le Roux P, Nishimura D, Macovski A. Parameter relations for the Shinnar-Le Roux selective excitation pulse design algorithm. *IEEE Trans Med Imaging*. 1991;10:53-65.
17. Boas MA. *Mathematical Methods in the Physical Sciences*. New York, NY, USA: John Wiley & Sons; second edition; 1983.
18. Oppenheim AV, Schafer RW. *Discrete-Time Signal Processing*. Englewood Cliffs, NJ, USA: Prentice Hall; 1989.
19. Strang G. *Introduction to Linear Algebra*, 4th edn. Wellesley, MA, USA– Cambridge Press; 2009.
20. Scherfgen D. Online Integral calculator. http://www.integral-calculator.com; 2016.
21. Hennig J, Scheffler K. Easy improvement in signal to noise in RARE sequences with low refocusing flip angles. *Magn Reson Med*. 2000;44:983-985.
22. Press WH, Teukolsky SA, Veterling WT, Flannery BP. *Numerical Recipes*, 3rd edn. Cambridge, UK: Cambridge University Press; 2007:502-507.
23. Busse RF, Brau ACS, Vu A, Michelich CR, Bayram E, Kijovski R, et al. Effects of refocusing flip angle modulation and view ordering in 3D Fast Spin Echo. *Magn Reson Med*. 2008;60:640-649.
24. Mugler JP, Kiefer B, Brookeman JR. Three-dimensional T2-weighted imaging of the brain using very long spin-echo trains. Proc. 8th Annual Meeting of the ISMRM, Denver, CO, USA; 2000. Abstract 687.
25. Zur Y, Chen W. A technique to eliminate artifacts in 3D fast spin echo imaging. Proc. Annual Meeting of the ISMRM, Milan, Italy; 2014. Abstract 1648.
26. Alsop DC. Phase insensitive preparation of single-shot rare: application to diffusion imaging in humans. *Magn Reson Med*. 1997;38:527-533.

27. Kingsley PB. Introduction to diffusion tensor imaging mathematics: part I. Tensors, rotations, and eigenvectors. *Concepts Magn Reson Part A* 2006;28A:101-122.

How to cite this article: Zur Y. Analysis of the multi-echo spin-echo pulse sequence. *Concepts Magn Reson Part A*. 2017;46A:e21402. https://doi.org/10.1002/cmr.a.21402

APPENDIX A

ANALYTIC EXPRESSION FOR M AFTER *n* RF PULSES

We derive an analytic expression for the magnetization $\mathbf{M^{(n)}}$ after n pulses with equal flip angles θ.

As shown in Figure 2, the angle between $\mathbf{V_A}$ (Equation (7)) and the z-axis is $\delta_1 = 90°$–angle(1, λ), and between $\mathbf{V_A}$ and the x-axis angle(1, λ). The first step in the calculation is the rotation of $\mathbf{M_P}$ and $\mathbf{M_A}$ clockwise around the y-axis by δ_1 radians (y points into the page), to align $\mathbf{M_A}$ (and $\mathbf{V_A}$) with the z-axis and $\mathbf{M_P}$ with the x-axis. From Figure 2:

$$\sin(\delta_1) = \sin[90° - \text{angle}(1,\lambda)] = \frac{1}{\sqrt{1+\lambda^2}} \tag{A1a}$$

$$\cos(\delta_1) = \sin[\text{angle}(1,\ \lambda)] = \frac{\lambda}{\sqrt{1+\lambda^2}} \tag{A1b}$$

After n pulses, $\mathbf{M_P}$ rotates by $n\psi$ radians in the clockwise direction around the z-axis which is aligned with $\mathbf{V_A}$. The full rotation operator $\mathbf{R^{(n)}}$ of $\mathbf{M_P}$ by the n RF pulses is a product of 3 rotation matrices: (i) a clockwise rotation, $\mathbf{R}(\delta_1)_y$, of $\mathbf{V_A}$ by δ_1 degrees around y to align $\mathbf{V_A}$ with the z-axis; (ii) a clockwise rotation $\mathbf{R}(n\psi)_z$ of M_P by $n\psi$ radians around the z-axis; (iii) a rotation $\mathbf{R}(-\delta_1)_y$ by $-\delta_1$ around y to restore $\mathbf{V_A}$ back to its original position.

$$\boldsymbol{R}^{(n)} = \boldsymbol{R}(-\delta_1)_y \cdot \boldsymbol{R}(n\psi)_z \cdot \boldsymbol{R}(\delta_1)_y = \begin{pmatrix} c_1c_2^2+s_2^2 & c_2s_1 & c_2s_2(1-c_1) \\ -c_2s_1 & c_1 & s_1s_2 \\ c_2s_2(1-c_1) & -s_1s_2 & c_1s_2^2+c_2^2 \end{pmatrix} \tag{A2}$$

where $s_2 \equiv \sin(\delta_1)$ and $c_2 \equiv \cos(\delta_1)$ are given by (A1) and $c_1 \equiv \cos(n\psi)$, $s_1 \equiv \sin(n\psi)$. From Equation (9b),

$$\exp(in\psi) = \cos(n\psi) + i\sin(n\psi) = \left[\exp\left(i\frac{\psi}{2}\right)\right]^{2n} = \left[C\cos(\phi) + iS\sqrt{1+\lambda^2}\right]^{2n}. \tag{A3}$$

From (A3), $c_1 = \cos(n\psi) = \text{real}[\exp(in\psi)]$ and $s_1 = sin(n\psi) = \text{imag}[\exp(in\psi)]$.

The clockwise rotation matrices in (A2) are[27]:

$$\boldsymbol{R}(\delta_1)_y = \begin{pmatrix} \cos(\delta_1) & 0 & -\sin(\delta_1) \\ 0 & 1 & 0 \\ \sin(\delta_1) & 0 & \cos(\delta_1) \end{pmatrix}; \quad \boldsymbol{R}(n\psi)_z = \begin{pmatrix} \cos(n\psi) & \sin(n\psi) & 0 \\ -\sin(n\psi) & \cos(n\psi) & 0 \\ 0 & 0 & 1 \end{pmatrix}. \tag{A4}$$

$\mathbf{R^{(n)}}$ in (A2) has no effect on $\mathbf{M_A}$, ie, $\mathbf{R}^{(n)}\boldsymbol{M_A} = \boldsymbol{M_A}$. The total magnetization $\mathbf{M^{(n)}}$ after n RF pulses is given by:

$$\boldsymbol{M}^{(n)} = \boldsymbol{R}^{(n)} \cdot \boldsymbol{M_i} = \boldsymbol{R}^{(n)} \cdot (\boldsymbol{M_A} + \boldsymbol{M_P}) = \boldsymbol{M_A} + \boldsymbol{M_P}^{(n)}. \tag{A5}$$

Where $\boldsymbol{M_P}^{(n)} = \boldsymbol{R}^{(n)} \cdot \boldsymbol{M_P}$.

$\mathbf{M_A}$ and $\mathbf{M_P}$ are given by Equation (10). Computing $\mathbf{M^{(n)}}$ with Equations (2-5) yield identical results to Equations (A2) and (A5).

APPENDIX B

FOURIER COEFFICIENTS OF PI-SYMMETRIC AND SYMMETRIC FUNCTIONS

A function $M(x)$ defined in the range $[-\pi,\ \pi]$ is pi-symmetric if

$$M(x) = M(x-\pi)$$

Or pi-antisymmetric if

$$M(x) = -M(x-\pi).$$

Similar to symmetric and antisymmetric functions, any function in $[-\pi,\ \pi]$ can be written as a sum of a pi-symmetric function and another pi-antisymmetric function (reference (17) page 322).

The Fourier coefficient A_n of a function $M(x)$ defined in $[-\pi,\ \pi]$ is given by

$$A_n = \frac{1}{2\pi}\int_{-\pi}^{\pi} M(x)e^{-inx}dx = \frac{1}{2\pi}\int_{-\pi}^{0} M(x)e^{-inx}dx + \frac{1}{2\pi}\int_{0}^{\pi} M(x)\cdot e^{-inx}dx \equiv I_A + I_B. \tag{B1}$$

In the first integral I_A, we substitute $x' = x - \pi$; if M is pi-symmetric

$$I_A = \frac{1}{2\pi}\int_{-\pi}^{0} M(x)\cdot e^{-inx}dx = \frac{1}{2\pi}\int_{0}^{\pi} M(x')\cdot e^{-inx'}e^{in\pi}dx'$$
$$= I_B \text{ for } n \text{ even}, \ -I_B \text{ for } n \text{ odd.} \quad \text{(B2a)}$$

If M is pi-antisymmetric

$$I_A = \frac{1}{2\pi}\int_{-\pi}^{0} M(x)\cdot e^{-inx}dx = \frac{-1}{2\pi}\int_{0}^{\pi} M(x')\cdot e^{-inx'}e^{in\pi}dx'$$
$$= I_B \text{ for } n \text{ odd}, \ -I_B \text{ for } n \text{ even.} \quad \text{(B2b)}$$

Consequently, if M is pi-symmetric, A_n is $2I_B$ for even n and 0 for odd n. If M is pi-antisymmetric, A_n is $2I_B$ for odd n and 0 for even n. Since the echo amplitude is A_0, pi-antisymmetric M will not contribute to the echo.

A symmetric (antisymmetric) function M_{sym} (M_{asym}) is defined by

$$M_{sym}(x) = M_{sym}(-x); \quad M_{asym}(x) = -M_{asym}(-x)$$

The Fourier coefficients $\{A_n\}_{sym}$ ($\{A_n\}_{asym}$) of a symmetric (antisymmetric) function $M_S(x)$ (M_A (x)) are (reference (17) chapter 7 section 9):

$$\{A_n\}_{sym} = \frac{1}{\pi}\int_0^{\pi} M_s(x)\cdot\cos(nx)dx;$$
$$\{A_n\}_{asym} = \frac{-i}{\pi}\int_0^{\pi} M_A(x)\cdot\sin(nx)dx. \quad \text{(B3)}$$

APPENDIX C

MATLAB FUNCTION TO CALCULATE ALL FOURIER COEFFICIENTS USING EQUATION (16)

The output matrices M_P and M_z contain $A_k^{(n)}$and $B_k^{(n)}$) for all k and all RF pulses n = 1-N.

```
function [Mp, Mz] = CalcFourier(Flips, T1, T2, esp)
% Calculate Fourier components for all RF pulses with relaxation using fft.
% input: Flips = vector of flip angles in degrees.
%     T1, T2 = relaxation times in msec.
%     esp = time between adjacent RF pulses, msec.
% output: Mp, Mz = matrices with all Fourier components of Mxy and Mz.
% ==================================================
% initialize variables.
NRF = length(Flips);   % number of RF pulses.
mp = 1;   % initial mp is 1.
mz = 0;   % initial mz = 0.
T2 = min(T1, T2);
N = 4*NRF + 1;
Mp = zeros(N, NRF);   % initialize Mp matrix
Mz = zeros(N, NRF);   % initialize Mz matrix
a = cosd(Flips/2);   % alpha of x RF pulses.
b = 1j*sind(Flips/2);   % beta of x RF pulses.
E1 = exp(-esp/(2*T1));
E2 = exp(-esp/(2*T2));
z = exp(1j*(0:N - 1)*2*pi/N).;   % N equally spaced angles.

c1 = conj(a).*b;
c2 = abs(a).^2 - abs(b).^2;
c3 = conj(a).*conj(b);

% loop through all RF pulses.
for j = 1:NRF;
mp1 = (E2*conj(z)*conj(a(j))).^2.*mp - E2^2*b(j)^2*conj(mp)...
+ 2*E1*E2*c1(j)*conj(z).*mz + 2*E2*conj(z)*(1 - E1)*c1(j);
mz = -2*E2*E1*real(c3(j)*conj(z).*mp) + E1^2*c2(j)*mz + (1 - E1)*(E1*c2(j) + 1);
mp = mp1;
Mp(:, j) = mp;
Mz(:, j) = mz;
end;

% Fourier transform.
Mp = fftshift(fft(Mp), 1)/N;
Mz = fftshift(fft(Mz), 1)/N;
```

APPENDIX D

CALCULATION OF THE ECHO AMPLITUDE OF THE HENNIG-SCHEFFLER MULTI-SPIN-ECHO SEQUENCE

In this Appendix, we calculate the integral $\boldsymbol{I}^{(n)}$ in Equation (17b) for the Hennig and Scheffler sequence,[21] where the flip angle θ_1 of the first periodic operator is $\theta_1 = 90° + \theta/2$. $\boldsymbol{I}^{(n)}$ in (17b) is the contribution of the rotating magnetization $\mathbf{M_P}$ to the echo. We use $\mathbf{R^{(n)}}$ in Equation (A2) to calculate it, as we did in Equation (32).

The initial magnetization $\mathbf{M_i} = [M_{ix}, M_{iy}, M_{iz}]^T$ and the pseudo steady-state magnetization $\mathbf{M_A}$ of this sequence are given by (21) and (22). From Equation (10), the x, y, and z components of $\mathbf{M_P}$ are:

$$M_{Px} = \frac{-\lambda M_{iz} + \lambda^2 M_{ix}}{1+\lambda^2}; \quad M_{Py} = M_{iy}; \quad M_{Pz} = \frac{-M_{Px}}{\lambda}. \quad \text{(D1)}$$

The relation between θ and θ_1 are given by Equation (23), ie, $\cos(\theta_1)\frac{\cos(\frac{\theta}{2})}{\sin(\frac{\theta}{2})} = -\sin(\theta_1)$. Using this relation and substituting $\mathbf{M_i}$ (Equation (21)) into (D1), we can write $\mathbf{M_P}$

in terms of the flip angles and ϕ:

$$M_{Px} = 2C_0^2 \cdot \frac{\lambda^2 cos^2(\phi)}{1+\lambda^2}; \quad M_{Py} = -C_0^2 \cdot \sin(2\phi); \quad M_{Pz} = \frac{-M_{Px}}{\lambda} \tag{D2}$$

where $C_0 = \cos\left(\frac{\theta_1}{2}\right)$.

To find $\mathbf{M_P^{(n)}}$, the contribution of $\mathbf{M_P}$ to the echo, we multiply $\mathbf{M_P}$ by $\mathbf{R^{(n)}}$ (Equation (A5)), ie, we substitute $\mathbf{M_P}$ in (D2) into Equation (32). The imaginary part (Equation (32b)) is

$$\mathrm{Im(echo)}_{MP} = \frac{1}{2\pi}\int_{-\pi}^{\pi}(-c_2 s_1 \cdot M_{px} + s_1 s_2 \cdot M_{pz} + c_1 \cdot M_{py})\, d\phi = 0 \tag{D3}$$

where $s_2 = \sin(\delta_1)$ and $c_2 = \cos(\delta_1)$ are given by (A1a) and (A1b), $c_1 = \cos(n\psi)$ and $s_1 = \sin(n\psi)$ are given by (A3). All the terms in (D3) are antisymmetric in ϕ and vanish in the integration.

The real part (Equation (32a)) is:

$$\mathrm{Re(echo)}_{MP} = \frac{1}{2\pi}\int_{-\pi}^{\pi}\left[\left(c_1 c_2^2 + s_2^2\right) \cdot M_{px} + c_2 s_2 (1 - c_1) \cdot M_{pz} + M_{py} \cdot c_2 s_1\right] d\phi. \tag{D4}$$

To evaluate (D4), we substitute (D2) into (D4). The result is

$$\boldsymbol{I^{(n)}} = \mathrm{Re(echo)}_{MP} = \frac{1}{2\pi}\int_{-\pi}^{\pi} 2C_0^2 \cdot \left[c_2^2 c_1 \cdot cos^2(\phi) - c_2 s_1 \cdot \sin(\phi)\cos(\phi)\right] d\phi. \tag{D5}$$

From the definitions of c_2, c_1, and s_1:

$$\boldsymbol{I^{(n)}} = \frac{C_0^2}{\pi} \cdot \left\{ \int_{-\pi}^{\pi} \frac{\lambda^2}{1+\lambda^2}\cos^2(\phi) \cdot \cos(n\psi) d\phi - \int_{-\pi}^{\pi} \frac{\lambda}{\sqrt{1+\lambda^2}} \frac{\sin(2\phi)}{2} \sin(n\psi) d\phi \right\}. \tag{D6}$$

Both integrals in (D6) do not have an analytic solution, but can be easily calculated by numerical integration. The full echo amplitude is (Equations (17b) and (24b)):

$$\mathrm{Echo}(n) = \mathcal{A}_0 + I^{(n)} = S + S\frac{1-S}{1+S} + I^{(n)} \tag{D7}$$

As explained above in Equation (25), the amplitude of the first echo is $S_0^2 = \sin^2\left(\frac{\theta_1}{2}\right)$. The echo in (D7) with $n = 1$ is the second acquired echo.